



Trans. Nonferrous Met. Soc. China 35(2025) 3357–3367

Transactions of Nonferrous Metals Society of China

www.tnmsc.cn



# Improved resistance to creep and underlying mechanisms in TiB/(TA15-Si) composites with network structure

Shuai WANG<sup>1</sup>, Rui ZHANG<sup>1</sup>, Ming JI<sup>1</sup>, Feng-bo SUN<sup>1</sup>, Zi-shuo MA<sup>1</sup>, Qi AN<sup>1</sup>, Lu-jun HUANG<sup>1,2</sup>, Lin GENG<sup>1,2</sup>

- School of Materials Science and Engineering, Harbin Institute of Technology, Harbin 150001, China;
  State Key Laboratory of Precision Welding & Joining of Materials and Structures,
  - Harbin Institute of Technology, Harbin 150001, China

Received 25 February 2024; accepted 3 July 2024

**Abstract:** To assess the high-temperature creep properties of titanium matrix composites for aircraft skin, the TA15 alloy, TiB/TA15 and TiB/(TA15–Si) composites with network structure were fabricated using low-energy milling and vacuum hot pressing sintering techniques. The results show that introducing TiB and Si can reduce the steady-state creep rate by an order of magnitude at 600 °C compared to the alloy. However, the beneficial effect of Si can be maintained at 700 °C while the positive effect of TiB gradually diminishes due to the pores near TiB and interface debonding. The creep deformation mechanism of the as-sintered TiB/(TA15–Si) composite is primarily governed by dislocation climbing. The high creep resistance at 600 °C can be mainly attributed to the absence of grain boundary  $\alpha$  phases, load transfer by TiB whisker, and the hindrance of dislocation movement by silicides. The low steady-state creep rate at 700 °C is mainly resulted from the elimination of grain boundary  $\alpha$  phases as well as increased dynamic precipitation of silicides and  $\alpha_2$ .

**Key words:** discontinueously reinforced titanium matrix composite; TiB whisker; network structure; silicides; creep properties

# 1 Introduction

Discontinuously reinforced titanium matrix composites (DRTMCs) have attracted considerable attention due to the potential to meet the increasing demand for high-temperature properties, which can be challenging to achieve with a single titanium alloy [1–5]. In particular, HUANG et al [6] proposed a network structure design and successfully fabricated a series of quasi-continuous network-structured TMCs using a combination of the Hashin–Shtrikman (H–S) theory, low-energy ball milling and hot-pressing sintering. This approach enabled the control of the spatial distribution of TiB

whiskers within the matrix, transitioning from a conventional uniform distribution to a network distribution. This transformation greatly improved the ductility of DRTMCs [1,7–9]. Subsequently, introducing silicides into phase boundaries has further improved the high-temperature properties of these composites, leading to the development of two-scale network TMCs, such as (TiB+Ti<sub>5</sub>Si<sub>3</sub>)/Ti6Al4V and TiB/(TA15–Si) composites [7,10–12].

It is worth emphasizing that the creep properties play a vital role in assessing the thermal stability of structural assemblies made of TMCs during prolonged service periods [13]. Creep deformation is generally characterized as a slow plastic deformation occurring at high temperatures

(typically above  $0.3T_{\rm m}$ ) and under stresses lower than the yield strength [14]. The typical creep curve follows the three-stage theory, a most used creep theory until now. This theory includes the stages of deceleration creep, steady-state creep (where work hardening and thermal activation softening are balanced) and acceleration creep (characterized by the formation of micro defects and accumulation of damage).

The creep performance of TMCs is influenced by various factors. Apart from creep temperature and stress, the characteristics of the matrix, reinforcement and their interface also play a significant role in determining the creep properties. Studies have shown that TC4 alloys exhibited superior creep resistance compared to commercially pure titanium (CP-Ti) and even TiB/CP-Ti composites [15]. This can be attributed to the presence of the  $\alpha/\beta$  phase boundary in TC4 alloys, which impeded the slip of dislocations and grain boundaries. The mesh-basket or lamellar microstructure generally exhibited better creep resistance compared to bimodal and equiaxed microstructures in titanium alloys. Regarding the effect of reinforcement on creep performance, XIAO et al [16] investigated the creep behavior of (TiB+TiC+La<sub>2</sub>O<sub>3</sub>)/Ti composites and found a significant improvement in creep performance. BOEHLERT [17] discovered that TC4-1B (wt.%) produced via powder metallurgy can exhibit remarkable enhancements in creep resistance compared to TC4 alloy. During in-situ creep testing conducted at 455 °C and 450 MPa, preferential fracture of TiB whiskers can be observed within the composite. PRASAD et al [18] also reported enhanced creep resistance in IMI834 alloy after the introduction of 0.2 wt.% B and highlighted the load transfer strengthening effect of TiB whiskers. In addition, Si also played a crucial role in the creep properties of titanium alloys and TMCs. XU et al [19] and ZHENG et al [20,21] prepared hybrid  $(TiB+TiC+Y_2O_3)/Ti-6Al-4Sn-8Zr$ reinforced 0.8Mo-1W-1Nb-0.25Si composites through induction melting and extensively investigated the evolution of silicides. They found that silicides can hinder dislocation movement and pin the  $\alpha/\beta$  phase boundary, thereby improving the creep resistance of the composites. However, there is limited research on the creep behavior of near- $\alpha$  high-temperature titanium alloys with the addition of TiB and Si, and the corresponding creep deformation and creepresistant mechanisms are not yet fully understood.

In the present work, the high-temperature creep behavior of TiB/(TA15-Si) composites with network structure was investigated in detail compared to TA15 alloy and TiB/TA15 composite. This study aimed to explore the mechanisms of creep deformation and resistance to creep, which can provide valuable insights for the long-term high-temperature applications of TMCs and other metal matrix composites.

# 2 Experimental

The fabrication processes of the as-sintered TiB/(TA15-Si) composite mainly included lowenergy ball milling and vacuum hot pressing sintering, which has been detailed in the previous work [11]. The spherical TA15 (Ti-6.5Al-2Zr-1Mo-1V) alloy powders with a large size range of 90-150 µm were raw materials as the matrix. TiB<sub>2</sub> powders (1-8 μm) and Si powders (2-3 μm) were raw materials as the reinforcement. According to the previously optimized compositions [11], the contents of TiB2 and Si powders were set at 2 wt.% (equivalent to 3.5 vol.% TiB) and 0.3 wt.%, respectively. All the matrix and reinforcement powders were first mixed, and then subjected to low-energy ball-milling (160 r/min, 5 h, 5:1, Ar atmosphere) and sintering (1300 °C, 2 h, 20 MPa, vacuum degree of  $10^{-2}$  Pa) in sequence. For comparison, the same preparation processes were used to fabricate the monolithic TA15 alloy and 3.5 vol.% TiB/TA15 composite.

The microstructural characteristics were analyzed using optical microscopy, scanning electron microscopy (SEM, ZEISS SUPRA 55 SAPPHIRE) and transmission electron microscopy (TEM, FEI Talos F200x). Metallographic samples were prepared by grinding, mechanical polishing and etching using Kroll's solution (5 vol.% HF + 15 vol.% HNO<sub>3</sub> + 85 vol.% H<sub>2</sub>O). TEM samples were thinned by grinding and ion-milling to produce 3 mm-diameter discs with an electron transparent region. High-temperature creep tests were carried out on the RWS50 testing machine equipped with load and displacement sensors. The creep behavior of the alloy and composites was evaluated at temperatures of 600 and 700 °C. Specifically, the applied creep stresses were 150,

200 and 250 MPa at 600 °C as well as 100, 110, 120 and 140 MPa at 700 °C. The relevant gauge dimensions of the samples were 10 mm × 5 mm × 2 mm, and the creep data were recorded with an interval of 20 s. It is worth noting that the creep tests were designed to be interrupted if the samples did not fracture within 100 h of testing.

#### 3 Results and discussion

#### 3.1 Microstructure characteristics

The microstructural characteristics of the as-sintered TA15 alloy, 3.5vol.%TiB/TA15 and 3.5vol.%TiB/(TA15–Si) composites are shown in Fig. 1. The TA15 alloy exhibits a typical Widmannstatten microstructure, with continuous and brittle grain boundary  $\alpha$  phases ranging in width from 3 to 10  $\mu$ m as shown in Figs. 1(a, b).

This microstructural feature is known to be detrimental to the ductility and toughness of titanium alloys and composites [22]. The  $\alpha$  colonies in the TA15 alloy consist of fine lamellar  $\alpha$  and residual  $\beta$  phases. In contrast, the introduction of TiB reinforcement in the as-sintered 3.5vol.%TiB/ TA15 composite leads to the formation of ceramic TiB phases at the prior  $\beta$  grain boundaries, as shown in Figs. 1(c, d). This microstructural helps evolution to eliminate the coarse Widmannstatten microstructure and continuous grain boundary  $\alpha$  phase, which is consistent with previous reports in the literature [23]. Additionally, the quasi-continuous network-structured TiB can refine the prior  $\beta$  phase. This special microstructure constructs a bi-connectivity of the matrix-matrix whisker-whisker phases, providing increased space for dislocation movement. Further

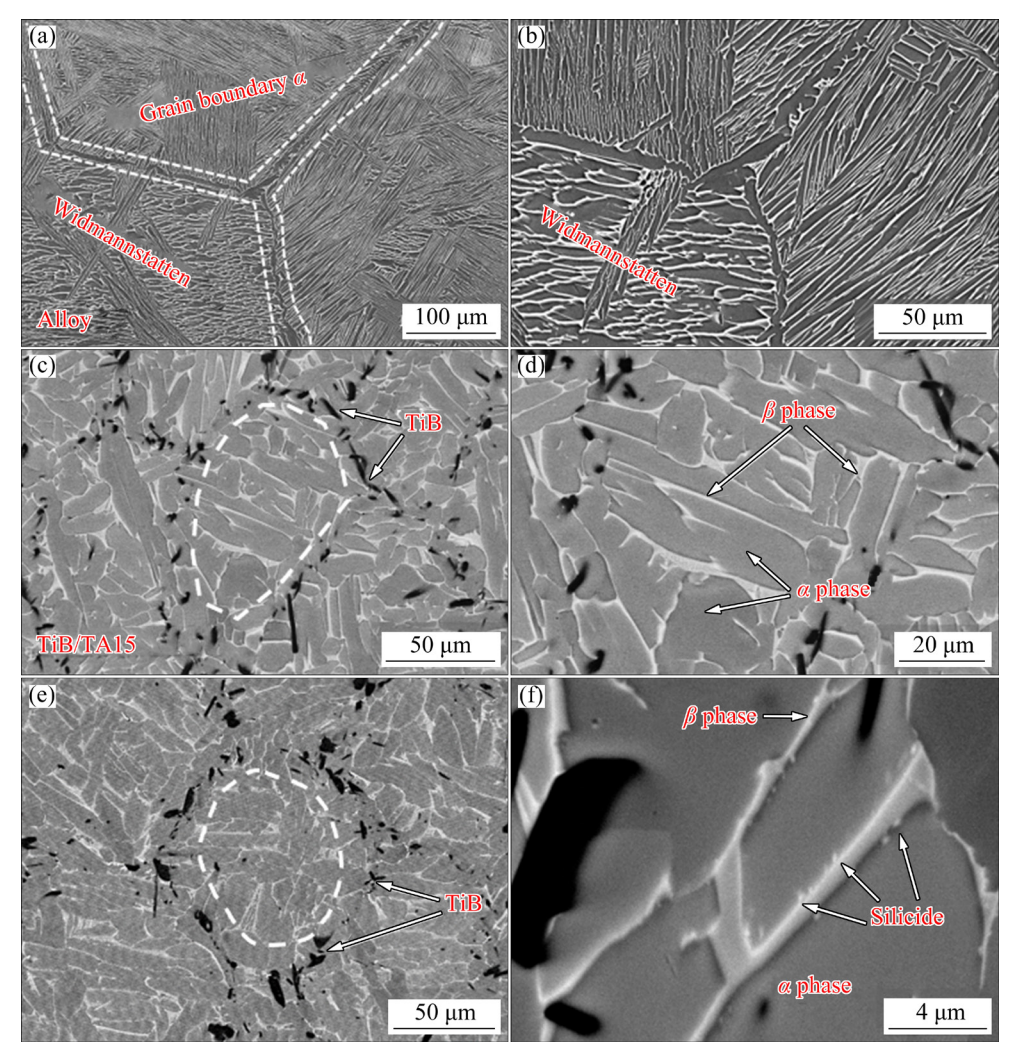
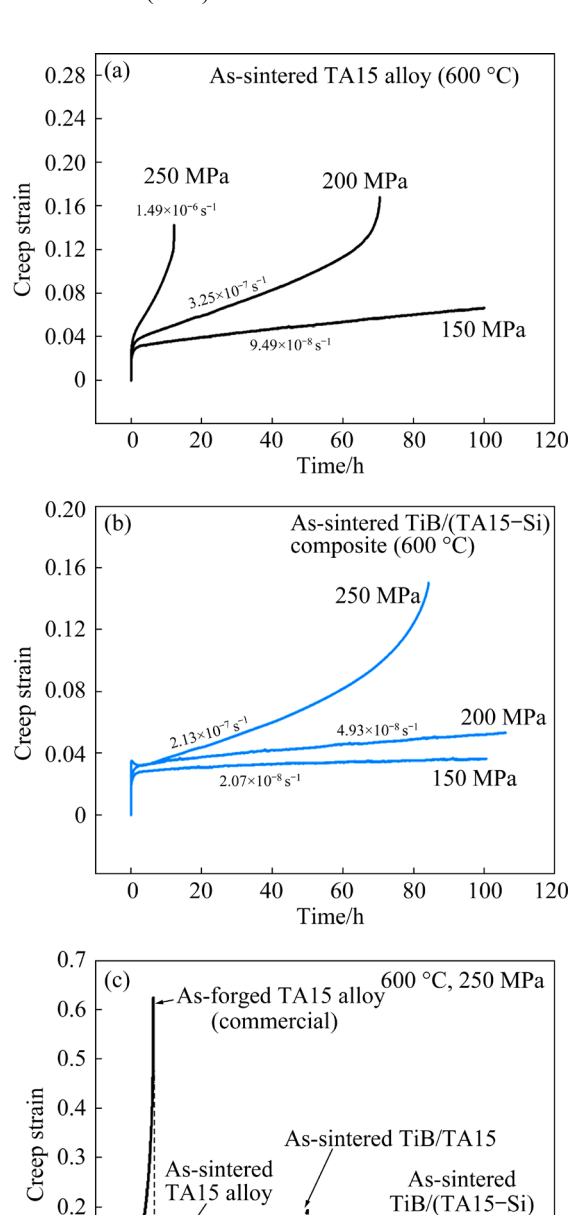


Fig. 1 Microstructures of as-sintered TA15 alloy (a, b), 3.5vol.%TiB/TA15 (c, d) and 3.5vol.%TiB/(TA15–Si) (e, f) composites: (a) Low-magnification Widmannstatten structure; (b) High-magnification Widmannstatten structure; (c, e) Network structure; (d) Matrix inside network; (f) Matrix and silicides inside network

addition of Si in the as-sintered TiB/(TA15–Si) composite mainly promotes the precipitation of silicides along the  $\alpha/\beta$  phase boundaries, as shown in Figs. 1(e, f). During the hot-pressing sintering process, the formation of sub-micro silicides involves complex processes, including in-situ reaction, high-temperature solid solution and diffusion, as well as heterogeneous nucleation and reprecipitation [24]. Notably, little addition of Si element does not significantly affect the network size of TiB or the grain size of lamellar  $\alpha$ .

# 3.2 Creep properties

To evaluate the thermal stability of as-sintered TMCs, creep tests were conducted and analyzed. Figure 2 shows the creep strain-time curves of assintered TA15 alloy and as-sintered TiB/(TA15-Si) composite at a creep temperature of 600 °C, along with a comparison of various materials. The corresponding creep performance indices are listed in Table 1. Under a creep stress of 150 MPa, the as-sintered alloy remains in the steady-state creep stage after 100 h, as shown in Fig. 2(a), with a steady-state creep rate of 9.49×10<sup>-8</sup> s<sup>-1</sup>. However, when the creep stress is increased to 200 MPa, the as-sintered alloy exhibits a significant decrease in creep property. The creep rupture life decreases to only 70.36 h, and the steady-state creep rate increases to  $3.25 \times 10^{-7} \,\mathrm{s}^{-1}$ . Furthermore, when the creep stress is increased to 250 MPa, the steadystate creep rate of the as-sintered alloy directly increases by an order of magnitude to 1.49×10<sup>-6</sup> s<sup>-1</sup>. As a result, the creep rupture life is sharply reduced to 12.16 h, and the duration of the steady-state creep stage is considerably shortened, indicating a high susceptibility of the as-sintered alloy to high-stress conditions. In contrast, the as-sintered TiB/(TA15-Si) composite exhibits superior creep performance. As shown in Fig. 2(b), when the creep stress is 150 MPa, the steady-state creep rate of the composite is  $2.07 \times 10^{-8} \,\mathrm{s}^{-1}$ , an order of magnitude lower than that of the as-sintered alloy. As the creep stress increases to 200 MPa, the steady-state creep rate of the composite only increases to  $4.93 \times 10^{-8} \,\mathrm{s}^{-1}$ , which is still an order of magnitude lower than that of the as-sintered alloy. When the creep stress increases to 250 MPa, the as-sintered composite exhibits a creep rupture life of 84.17 h, which is 6 times higher than that of the as-sintered alloy, as shown in Fig. 2(c). The steady-state creep rate is



**Fig. 2** Creep strain—time curves of as-sintered TA15 alloy (a) and TiB/(TA15—Si) composites (b) under condition of 600 °C and 150—250 MPa; Creep strain—time curves of various alloy and composites under condition of 600 °C and 250 MPa (c)

40

Time/h

13×10<sup>-7</sup>

20

Stage II

Stage III

80

100

0.1

0

 $2.13 \times 10^{-7} \, \mathrm{s}^{-1}$ , still an order of magnitude lower than that of the alloy. Notably, the creep performance of the as-sintered composite at 250 MPa is slightly higher than that of the alloys at 200 MPa, suggesting that the addition of TiB and silicides can significantly improve the creep performance of TA15 near- $\alpha$  high-temperature titanium alloy.

**Table 1** Creep properties of as-sintered alloy and composites under condition of 600 °C and 150–250 MPa

Material	Stress/ MPa	Steady creep rate/s <sup>-1</sup>	Time/h	Strain
	150	$9.49 \times 10^{-8}$	>100	0.066
As-sintered TA15 alloy	200	$3.25 \times 10^{-7}$	70.36	0.174
17115 anoy	250	$1.49 \times 10^{-6}$	12.16	0.144
As-sintered TiB/TA15 composite	250	5.02×10 <sup>-7</sup>	42.18	0.192
As-sintered	150	$2.07 \times 10^{-8}$	>100	0.036
TiB/(TA15-Si)	200	$4.93 \times 10^{-8}$	>100	0.050
composite	250	$2.13 \times 10^{-7}$	84.17	0.147

To analyze the roles of TiB and silicide individually, the as-sintered TiB/TA15 composite was obtained by the same fabrication process and tested at the creep condition of 600 °C and 250 MPa, as shown in Fig. 2(c). Obviously, the introduction of TiB can improve the creep performance of the as-sintered alloy and lead to a more prolonged steady-state creep stage. Specifically, the creep rupture life of 42.18 h is 2.5 times higher than that of the as-sintered alloy, and the steady-state creep rate of  $5.02 \times 10^{-7} \,\mathrm{s}^{-1}$  is 0.5 order of magnitude lower than that of the alloy. After introducing the Si, the creep property is further improved on the basis of TiB/TA15 as-sintered composite. The TiB/(TA15-Si) composite with the highest creep rupture life at 600 °C and 250 MPa also corresponds to the lowest steady-state creep rate (2.13×10<sup>-7</sup> s<sup>-1</sup>), which is 0.5 order of magnitude lower than that of the as-sintered TiB/TA15 composite and one order of magnitude lower than that of the as-sintered alloy. Additionally, the commercially forged TA15 alloy is also added for a comparison. Under the creep condition of 600 °C and 250 MPa, the forged TA15 alloy exhibits the lowest creep rupture life (6.17 h), the highest steady-state creep rate  $(7.05 \times 10^{-6} \, \text{s}^{-1})$ and the highest creep strain (0.62), as shown in Fig. 2(c). This indicates a low resistance to creep deformation and the steady-state creep stage cannot be significantly observed, suggesting that the creep parameters are already considered dangerous temperature and stress conditions for the forged alloy. As mentioned above, the creep rupture lives of both as-sintered alloy and composites decrease monotonically at 600 °C as the creep stress

increases. The steady-state creep rate also increases monotonically. This can be attributed to the fact that higher creep stress can promote dislocation slip, leading to increased creep deformation.

The creep properties of the alloy and composites at 700 °C are shown in Fig. 3 and Table 2. As presented in Fig. 3(a), the commercially forged alloy exhibits the lowest creep rupture life (2.24 h) and the highest steady-state creep rate  $(6.57 \times 10^{-5} \,\mathrm{s}^{-1})$ . In comparison, the as-sintered alloy possesses a creep rupture life of 20.44 h and a steady-state creep rate of  $1.80 \times 10^{-6} \,\mathrm{s}^{-1}$ . The as-sintered TiB/TA15 composite shows a similar creep performance, with a creep rupture life of 20.38 h and a steady-state creep rate of  $2.15 \times 10^{-6}$  s<sup>-1</sup>. This indicates that the introduction of TiB no longer improves the creep rupture life or reduce the steady-state creep rate of the alloy under the creep condition of 700 °C and 100 MPa. In contrast, the as-sintered TiB/(TA15-Si) composite exhibits superior creep performance at 700 °C. The creep rupture life is 109.32 h, which is 4.3 times

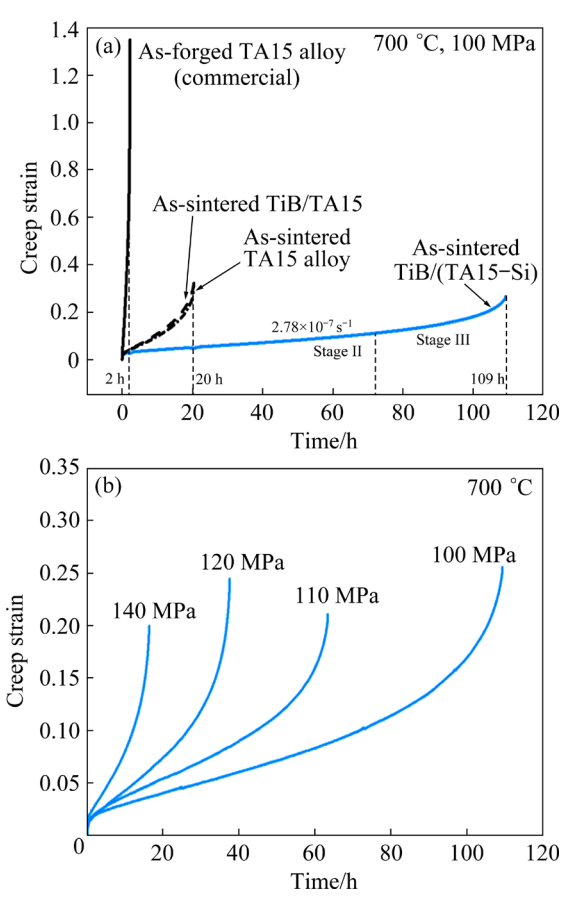


**Fig. 3** Creep strain—time curves at 700 °C: (a) Various alloy and composites under creep stress of 100 MPa; (b) As-sintered TiB/(TA15—Si) composites under different creep stresses

Table	2	Creep	properties	of	as-sintered	alloy	and
compo	site	es at 700	) °C				

Material	Stress/ MPa	Steady creep rate/s <sup>-1</sup>	Time/h	Creep strain
As-sintered TA15 alloy	100	$1.80 \times 10^{-6}$	20.44	0.325
As-sintered TiB/TA15 composite	100	2.15×10 <sup>-6</sup>	20.38	0.322
	100	$2.78 \times 10^{-7}$	109.32	0.261
As-sintered	110	$4.79 \times 10^{-7}$	63.32	0.217
TiB/(TA15-Si)	120	$8.07 \times 10^{-7}$	37.47	0.244
	140	$1.71 \times 10^{-6}$	16.28	0.202

higher than that of the alloy. And the steady-state creep rate is 2.78×10<sup>-7</sup> s<sup>-1</sup>, approximately an order of magnitude lower than that of the alloy. This suggests that the introduction of Si can continue to play a significant role in strengthening at 700 °C. As shown in Fig. 3(b), as the creep stress increases, the steady-state creep rate of as-sintered composites increases rapidly and the creep rupture life decreases rapidly. Under a creep stress of 140 MPa, the composite exhibits a steady-state creep rate of  $1.71 \times 10^{-6} \,\mathrm{s}^{-1}$  and a creep rupture life of 16.28 h, indicating that the creep properties of the composites at elevated temperatures are highly sensitive to stress. This behavior is mainly due to the increased thermal activation of atoms at higher temperatures, which reduces the resistance to dislocation motion within the crystal lattice.

# 3.3 Creep-resistant mechanisms

In the study of creep behavior of materials, the creep constitutive equation is a crucial relationship, which is expressed in Eq. (1):

$$\dot{\varepsilon} = A\sigma^n \exp\left[-Q/(RT)\right] \tag{1}$$

where  $\dot{\varepsilon}$  is the steady-state creep rate, A is the constant,  $\sigma$  is the creep stress, n is the creep stress exponent, Q is the creep activation energy, R is the molar gas constant and T is the creep temperature.

Taking the logarithm of both sides of this equation, the variant formula can be written in Eq. (2):

$$\ln \dot{\varepsilon} = \ln A - \frac{Q}{RT} + n \ln \sigma \tag{2}$$

When the temperature is fixed,  $\ln \dot{\varepsilon}$  is linearly related to  $\ln \sigma$  and the slope (that is to creep stress

exponent) can be obtained through linear fitting [25]. Then, the dominant creep deformation mechanism of the material can be inferred from the stress exponent. For simple alloys, when n is 1, the creep deformation belongs to the diffusion creep or Harper–Dom (H–D) creep. In this case, the diffusion creep can be further classified into Coble creep and Nabarro–Herring (N–H) creep. When n reaches 2, it indicates that grain boundary slip begins to play a role in the creep deformation of the material or serves as a part of the creep mechanism. When dislocation creep dominates in pure metals and some alloys, the creep stress exponent typically ranges from 3 to 5.

As mentioned above, the creep stress exponent can be obtained by fitting the creep constitutive equation, which indicates the growth rate of the steady-state creep rate with increasing creep stress (at a fixed creep temperature). A higher stress exponent implies a faster growth of steady-state creep rate, suggesting a more pronounced effect of stress on the creep rate. Therefore, the creep stress exponent can be used to determine the dominant creep deformation mechanism of the material. Figure 4 shows the steady-state creep rate-stress curves of as-sintered TA15 alloy and TiB/(TA15-Si) composites at different creep temperatures. All stress exponents are between 3 and 6, which indicates that the creep deformation mechanism is mainly the dislocation creep mechanism [16]. When the dislocation slip is blocked, the edge-type dislocations can be thermally activated to climb into the neighboring glide plane to continue to slip. This climbing process can relieve the stress concentration generated by the dislocation pile-up,

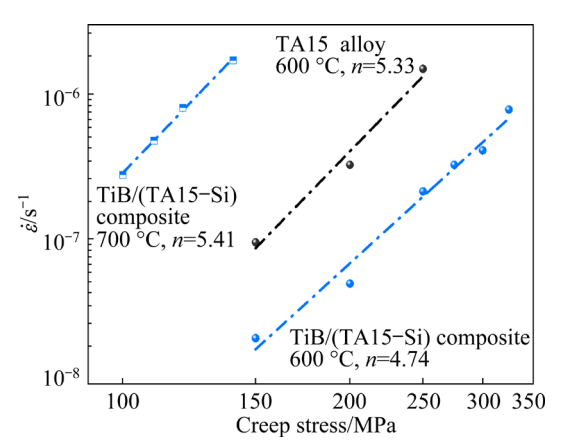


**Fig. 4** Steady-state creep rate—creep stress curves of as-sintered TA15 alloy and TiB/(TA15–Si) composites at different creep temperatures

including the cancellation of positive and negative edge dislocation. Specifically, the creep stress exponents of as-sintered TA15 alloy and TiB/(TA15–Si) composite are 5.33 and 4.74 when the creep temperature is 600 °C. After increasing the creep temperature to 700 °C, the creep stress exponent reaches 5.41. Overall, the creep stress exponents and stress sensitivities of the composite show an increasing trend with increasing creep temperature.

Figure 5 shows the post-creep microstructure of the as-sintered alloy and as-sintered TiB/ (TA15-Si) composite under a creep condition of 600 °C and 250 MPa. As shown in Fig. 5(a), some microcracks tend to appear at the grain boundaries in the as-sintered alloy, which is mainly due to grain boundary cracking caused by the uncoordinated deformation and stress concentration at a higher Figures 5(b-d) show stress. the post-creep microstructures of the as-sintered composite. The cracks mainly appear in the TiB whiskers, indicating that the TiB reinforcement can still effectively transfer the load during the creep process. Moreover, under this stress temperature condition, some pores also occur near the TiB whiskers due to interface debonding phenomena. GE et al [26] pointed out that the interface between the borides and matrix is usually prone to becoming a nucleation location for creep

cracks. Figure 5(d) shows the silicides at the  $\alpha/\beta$ phase boundaries in the as-sintered composite, which are capable of hindering dislocation motion during the creep process. Figure 6 shows the creep microstructures of as-sintered alloy and composite under a creep condition of 700 °C and 100 MPa. As shown in Fig. 6(a), the as-sintered alloy still exhibits pores at the grain boundaries due to stress concentration. These defects can grow and even lead to fracture of the material when the pores exceed the critical size in the subsequent process. In the as-sintered TiB/(TA15-Si) composite, the fracture phenomenon of the TiB whisker is no longer obvious, indicating a significant decline in load transfer strengthening. Furthermore, more creep pores begin to form at the TiB/Ti interfaces, as shown in Fig. 6(b), due to more severe deformation incongruity between the TiB and matrix at a higher temperature. LIU et al [27] and XU et al [28] also found this phenomenon in the creep deformation research of TMCs. Therefore, it is difficult for the TiB whiskers to play an effective strengthening role at a creep temperature of 700 °C. Meanwhile, the number of silicides at the  $\alpha/\beta$ -phase interface increases significantly, as shown in Figs. 6(c, d), which is attributed to the sufficient thermal activation and creep time. The increased silicides can further hinder the dislocation motion and improve the creep resistance of the composites.

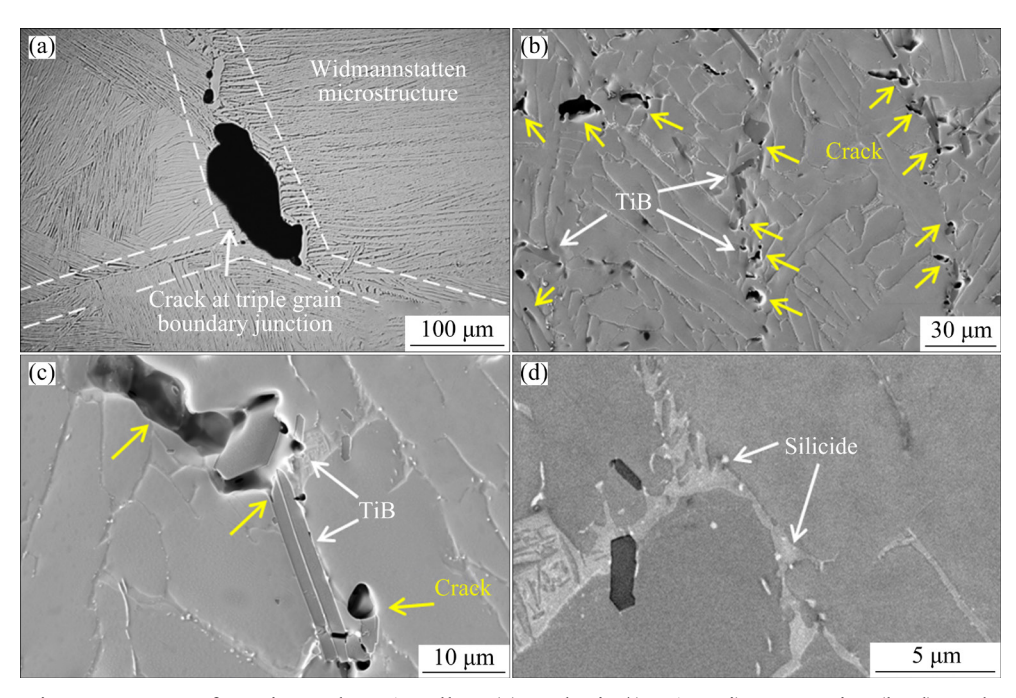


Fig. 5 Creep microstructures of as-sintered TA15 alloy (a) and TiB/(TA15-Si) composite (b-d) under condition of 600 °C and 250 MPa

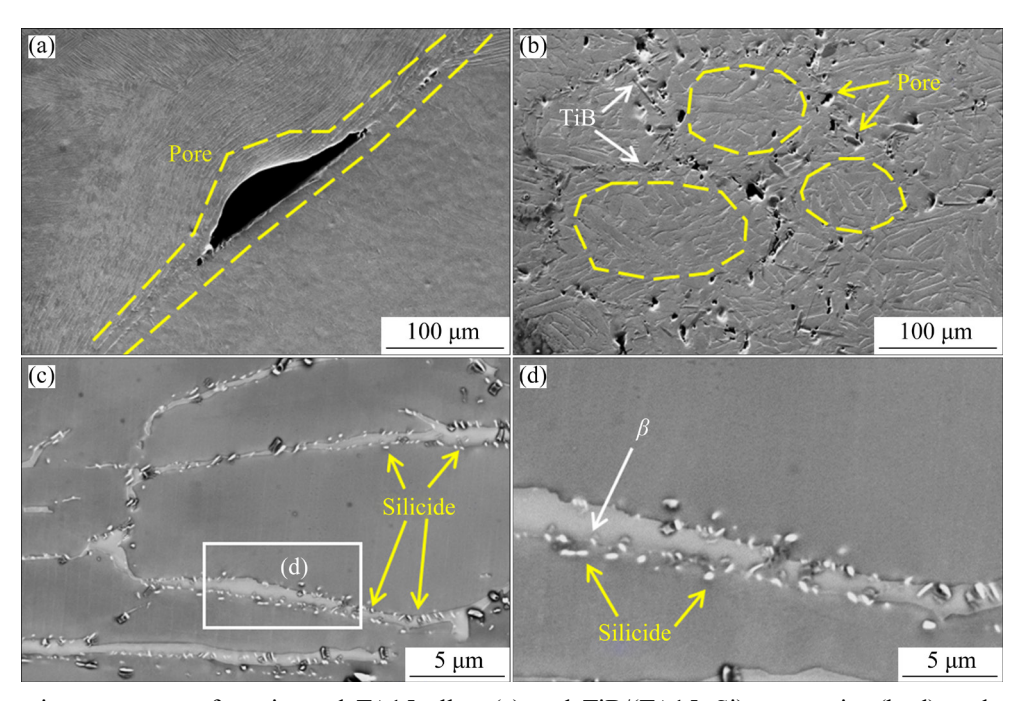


Fig. 6 Creep microstructures of as-sintered TA15 alloy (a) and TiB/(TA15-Si) composite (b-d) under condition of 700 °C and 100 MPa

By combining the characteristics of creep curves with creep microstructure, the creep-resistant mechanisms of the composites can be analyzed. For the as-sintered TA15 alloy, the microcracks are prone to preferentially nucleating at the brittle continuous grain boundary  $\alpha$  phase and expand under intense stress concentration, which ultimately leads to the creep fracture of the alloy. To improve the creep performance, TiB reinforcement is introduced into the TA15 alloy via powder metallurgy, resulting in a network-structured TiB/TA15 composite with a refined microstructure. Under a creep condition of 600 °C and 250 MPa, the as-sintered TiB/TA15 composite demonstrates superior creep performance compared to the as-sintered alloy. This is attributed to the effective load transfer strengthening by TiB reinforcement at this temperature. However, when the creep temperature is further elevated to 700 °C, both the composite and the alloy exhibit a similar level of creep resistance. At the higher temperature of 700 °C, the significant matrix softening leads to uncoordinated deformation and debonding at the TiB/Ti interface, thereby weakening the strengthening effect of the TiB reinforcement in the composite to the level of the as-sintered alloy. To further enhance the creep resistance, Si is added to the TiB/TA15 composite, resulting in the

TiB/(TA15-Si) composite. The silicides introduced at the  $\alpha/\beta$  phase interfaces can provide a significant strengthening. Especially, the strengthening effect of Si addition can be maintained at 700 °C, presenting high thermal stability for the creep performance of TiB/(TA15-Si) composite. The strengthening mechanisms of the Si-containing composite can be attributed to the dual effects of the solid solution Si atoms and the precipitated silicides. The solid solution Si atoms can impede the dislocation motion by pinning the dislocations through the strong interaction, while the silicide particles can act as a secondary phase to hinder the dislocation motion. ZHENG et al [21] also pointed out that the reinforcements such as TiB, silicides and La<sub>2</sub>O<sub>3</sub> can improve the creep performance of near- $\alpha$  titanium matrix composites by hindering dislocation motion. Additionally, the silicide/matrix interface is more stable compared to the TiB/Ti interface, which makes it difficult to form obvious microcracks during the creep process.

The TEM microstructure of the as-sintered TiB/(TA15–Si) composite after creep fracture under condition of 700 °C and 100 MPa is shown in Fig. 7. The EDS mapping of Mo, Si and Zr elements in Fig. 7(a) reveals that silicides begin to precipitate in the  $\alpha$  phases during the prolonged creep process. As shown in Figs. 7(b–d), obvious ordered  $\alpha_2$  solid

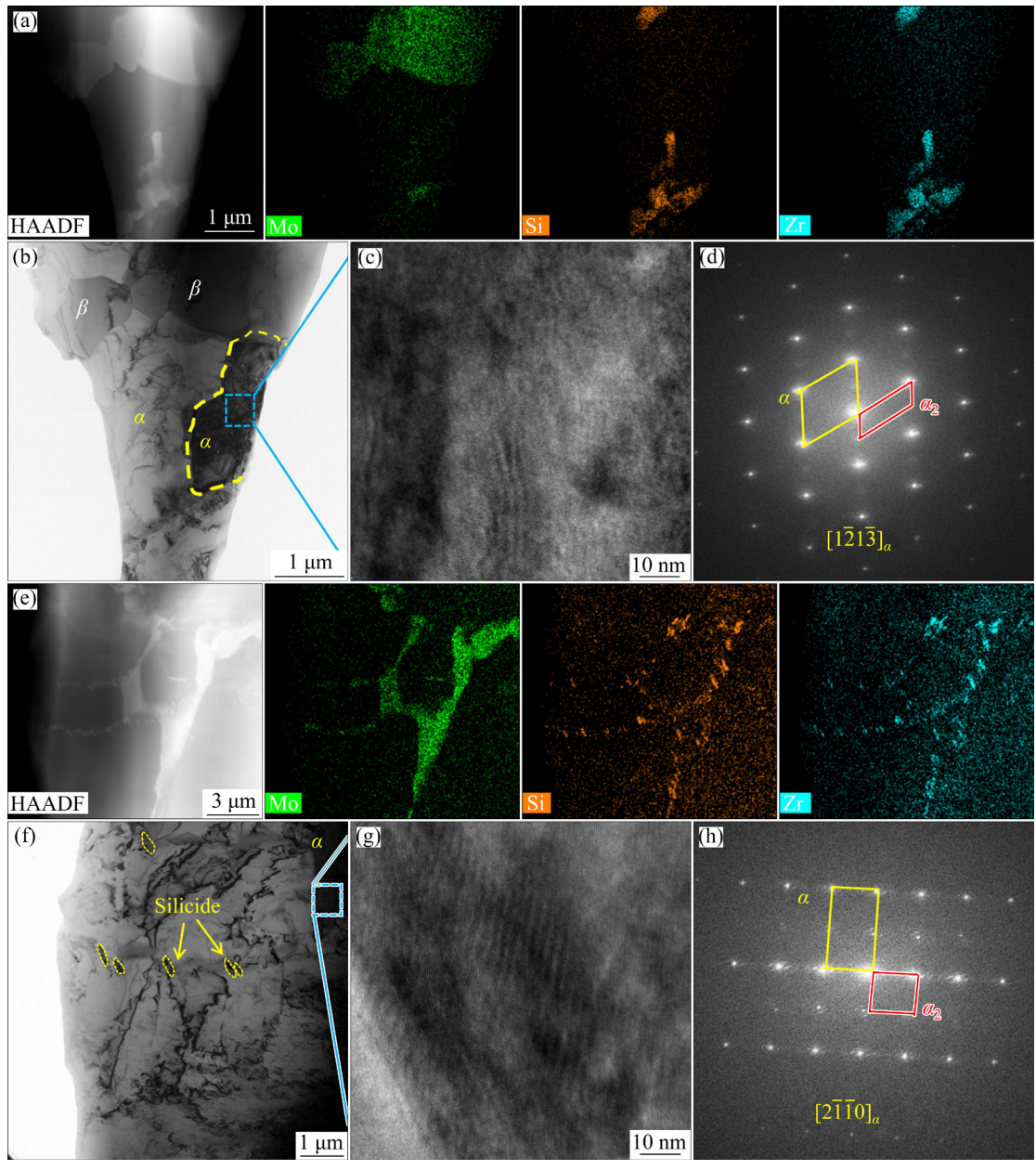


Fig. 7 Post-creep TEM morphologies of as-sintered TiB/(TA15-Si) composite under creep condition of 700 °C and 100 MPa: (a) HAADF and EDS mapping of silicides; (b) Bright-field image of (a); (c) HRTEM image of  $\alpha$  phase in (b); (d) FFT of (c); (e) HAADF and EDS mapping of increased silicides; (f) Bright-field image of (e); (g) HRTEM image of  $\alpha$  phase in (f); (h) FFT of (g)

solution phases are observed to precipitate within a part of the  $\alpha$  phases, as evidenced by the bright-field, high-resolution TEM and FFT results. Furthermore, a large number of new silicides are observed to precipitate along the phase interfaces during the creep process, as shown in Fig. 7(e) and the magnified image in Fig. 7(f). The distinctive needle-like silicides are consistent with the previously reported creep microstructure. The significant precipitation of  $\alpha_2$  is also observed, as shown in the high-resolution TEM and FFT results

in Figs. 7(g, h). The excellent creep performance of the as-sintered TiB/(TA15–Si) composite below 700 °C is mainly attributed to the combined effects of the silicides, load transfer of TiB and eliminated grain boundary  $\alpha$  phases. However, under the creep condition of 700 °C and 100 MPa, the TiB reinforcement is no longer able to provide effective strengthening. Instead, the increased precipitation of silicides and  $\alpha_2$  phase becomes the dominant factor contributing to the creep resistance. The newly precipitated second-phase particles,

including the silicides and  $\alpha_2$ , can provide a dynamic hindrance to the dislocation motion, thereby enhancing the creep performance of the as-sintered TiB/(TA15–Si) composite at the higher temperature of 700 °C. In summary, the absence of grain boundary  $\alpha$  phases and precipitation of more silicides and  $\alpha_2$  are the key microstructural factors responsible for the excellent creep performance of the as-sintered TiB/(TA15–Si) composite at 700 °C.

#### 4 Conclusions

- (1) The introduction of TiB and Si can both significantly improve the creep performance of the as-sintered TA15 alloy under a condition of 600 °C and 250 MPa. The addition of TiB leads to a 0.5-order-of-magnitude reduction in the steady-state creep rate compared to the alloy. Furthermore, the simultaneous addition of TiB and Si results in a one-order-of-magnitude reduction in the creep rate.
- (2) As the creep temperature increases to 700 °C, the load transfer of TiB whiskers declines due to interface debonding caused by matrix softening and uncoordinated deformation. However, the presence of silicides maintains a relatively stable improvement in creep performance within the temperature range of 600–700 °C.
- (3) According to the creep constitutive model, the dominant creep deformation mechanism in both as-sintered TA15 alloy and TiB/(TA15–Si) composites is dislocation creep at 600-700 °C. The as-sintered TiB/(TA15–Si) composite exhibits a significantly low steady-state creep rate, which can be mainly attributed to several key factors: the elimination of grain boundary  $\alpha$  phases, load transfer of TiB, and hindrance of dislocation movement by dynamic precipitation of silicides and  $\alpha_2$ .

# CRediT authorship contribution statement

Shuai WANG: Data curation, Writing — Original draft; Rui ZHANG: Supervision, Experimental assistance; Ming JI, Feng-bo SUN, Zi-shuo MA and Qi AN: Experimental assistance; Lu-jun HUANG: Conceptualization, Supervision; Lin GENG: Supervision.

#### **Declaration of competing interest**

The authors declare that they have no known competing financial interests or personal relationships

that could have appeared to influence the work reported in this paper.

#### **Acknowledgments**

This work was financially supported by the National Key R&D Program of China (No. 2022YFB3707405), the National Natural Science Foundation of China (Nos. U22A20113, 52171137, 52071116), Heilongjiang Provincial Natural Science Foundation, China (No. TD2020E001), and Heilongjiang Touyan Team Program, China.

### References

- [1] TJONG S C, MAI Y W. Processing-structure-property aspects of particulate- and whisker-reinforced titanium matrix composites [J]. Composites Science and Technology, 2008, 68(3/4): 583–601.
- [2] SINGH G, RAMAMURTY U. Boron modified titanium alloys [J]. Progress in Materials Science, 2020, 111: 100653.
- [3] ZHANG Xiang, ZHAO Nai-qin, HE Chun-nian. The superior mechanical and physical properties of nanocarbon reinforced bulk composites achieved by architecture design—A review [J]. Progress in Materials Science, 2020, 113: 100672.
- [4] ZHANG Fang-zhou, WANG Bo, CAO Qing-hua, ZHANG Li, ZHANG Hao-yang. Effect of deformation degree on microstructure and mechanical properties evolution of TiB<sub>w</sub>/Ti60 composites during isothermal forging [J]. Transactions of Nonferrous Metals Society of China, 2023, 33(3): 802–815.
- [5] HUANG Li-qing, HUANG Qun. High-strength Ti-BN composites with core-shell structured matrix and network-woven structured TiB nanowires [J]. Transactions of Nonferrous Metals Society of China, 2022, 32(4): 1169-1177.
- [6] HUANG Lu-jun, GENG Lin, PENG Hua-xin, ZHANG Jie. Room temperature tensile fracture characteristics of in situ TiBw/Ti6Al4V composites with a quasi-continuous network architecture [J]. Scripta Materialia, 2011, 64(9): 844–847.
- [7] HUANG Lu-jun, GENG Lin, PENG Hua-xin. Microstructurally inhomogeneous composites: Is a homogeneous reinforcement distribution optimal? [J]. Progress in Materials Science, 2015, 71: 93–168.
- [8] MORSI K, PATEL V V. Processing and properties of titanium-titanium boride (TiB<sub>w</sub>) matrix composites — A review [J]. Journal of Materials Science, 2007, 42(6): 2037–2047.
- [9] GUO Xiang-long, LU Wei-jie, WANG Li-qiang, QIN Ji-ning. A research on the creep properties of titanium matrix composites rolled with different deformation degrees [J]. Materials & Design, 2014, 63: 50-55.
- [10] JIAO Yang, HUANG Lu-jun, GENG Lin. Progress on discontinuously reinforced titanium matrix composites [J]. Journal of Alloys and Compounds, 2018, 767: 1196–1215.
- [11] WANG Shuai, HUANG Lu-jun, JIANG Shan, ZHANG Rui, LIU Bao-xi, SUN Feng-bo, AN Qi, JIAO Yang, GENG Lin. Microstructure evolution and tensile properties of as-rolled TiB/TA15 composites with network microstructure [J].

- Materials Science and Engineering A, 2021, 804: 140783.
- [12] HUANG Lu-jun, AN Qi, GENG Lin, WANG Shuai, JIANG Shan, CUI Xi-ping, ZHANG Rui, SUN Feng-bo, JIAO Yang, CHEN Xin, WANG Cun-yu. Multiscale architecture and superior high-temperature performance of discontinuously reinforced titanium matrix composites [J]. Advanced Materials, 2020, 33(6): 2000688.
- [13] HAYAT M D, SINGH H, HE Zhen, CAO Peng. Titanium metal matrix composites: An overview [J]. Composites Part A: Applied Science and Manufacturing, 2019, 121: 418–438.
- [14] ZHANG Bao-bing, TANG Y G, MEI Q S, LI Xiu-yan, LU Ke. Inhibiting creep in nanograined alloys with stable grain boundary networks [J]. Science, 2022, 378(6620): 659–663.
- [15] BARBOZA M J R, PEREZ E A C, MEDEIROS M M, REIS D A P, NONO M C A, NETO F P, SILVA C R M. Creep behavior of Ti–6Al–4V and a comparison with titanium matrix composites [J]. Materials Science and Engineering A, 2006, 428: 319–326.
- [16] XIAO Lv, LU Wei-jie, QIN Ji-ning, CHEN Yi-fei, ZHANG Di, WANG Min-min, ZHU Feng, JI Bo. Creep behaviors and stress regions of hybrid reinforced high temperature titanium matrix composite [J]. Composites Science and Technology, 2009, 69(11/12): 1925–1931.
- [17] BOEHLERT C J. The creep behavior of powder-metallurgy processed Ti-6Al-4V-1B(wt.%) [J]. Materials Science and Engineering A, 2009, 510/511: 434-439.
- [18] PRASAD K, SARKAR R, GHOSAL P, SATYANARAYANA D V V, KAMAT S V, NANDY T K. Tensile and creep properties of thermomechanically processed boron modified Timetal 834 titanium alloy [J]. Materials Science and Engineering A, 2011, 528: 6733– 6741.
- [19] XU Li-juan, ZHENG Yun-fei, LIANG Zhen-quan, XUE Xiang, HAN Shi-wei, XIAO Shu-long, TIAN Jing, CHEN Yu-yong. Effect of stress and temperature on creep behavior of a (TiB+TiC+Y<sub>2</sub>O<sub>3</sub>)/α-Ti composite [J]. Materials Characterization, 2021, 181: 111495.
- [20] ZHENG Yun-fei, XU Li-juan, CHEN Zhuo, WANG Xi-cheng, XUE Xiang, XIAO Shu-long, TIAN Jing, CHEN Yu-yong. Effects of hybrid reinforcements to the high

- temperature tensile and creep properties of a (TiB+TiC+ $Y_2O_3$ )/alpha-Ti composite [J]. Materials Characterization, 2022, 190: 112067.
- [21] ZHENG Yun-fei, XU Li-juan, YU Jian-xin, LIANG Zhen-quan, XUE Xiang, XIAO Shu-long, TIAN Jing, CHEN Yu-yong. Effect of TiB, TiC and Y<sub>2</sub>O<sub>3</sub> on tensile properties and creep behavior at 650 °C of titanium matrix composites [J]. Journal of Alloys and Compounds, 2022, 908: 164699.
- [22] YAN Zhi-bing, WANG Ke, ZHOU Yu, ZHU Xue-feng, XIN Ren-long, LIU Qing. Crystallographic orientation dependent crack nucleation during the compression of a Widmannstatten-structure α/β titanium alloy [J]. Scripta Materialia, 2018, 156: 110–114.
- [23] HUANG Li-guo, KONG Fan-tao, CHEN Yu-yong, XIAO Shu-long. Microstructure and tensile properties of Ti-6Al-4V-0.1B alloys of direct rolling in the near  $\beta$  phase region [J]. Materials Science and Engineering A, 2013, 560: 140–147.
- [24] MADSEN A, ANDRIEU E, GHONEM H. Microstructural changes during aging of a near-α titanium alloy [J]. Materials Science and Engineering A, 1993, 171: 191–197.
- [25] YANG Jian-hui, CHANG Ruo-han, GAO Peng, WEI Shi, LU Zi-chuan, YAO Cao-gen, XIAO Shu-long, CHEN Yu-yong. The creep behavior of (TiB+TiC+Y<sub>2</sub>O<sub>3</sub>)/alpha-Ti composites at high temperature and short-term [J]. Materials Characterization, 2022, 194: 112443.
- [26] GE Hua-long, LIU Gui-sen, ZHENG Shi-jian, YANG Ya-qian, LIU Kui, MA Xiu-liang. Dislocation climbing dominated decomposition and fracture of carbides in a Ni-based superalloy [J]. Acta Materialia, 2023, 246: 118669.
- [27] LIU D, ZHANG S Q, LI A, WANG H M. Creep rupture behaviors of a laser melting deposited TiC/TA15 in situ titanium matrix composite [J]. Materials & Design, 2010, 31(6): 3127–3133.
- [28] XU Li-juan, ZHENG Yun-fei, LIANG Zhen-quan, HAN Shi-wei, XUE Xiang, XIAO Shu-long, TIAN Jing, CHEN Yu-yong. Creep behavior and microstructure evolution of titanium matrix composites reinforced with TiB, TiC and Y<sub>2</sub>O<sub>3</sub> [J]. Transactions of Nonferrous Metals Society of China, 2023, 33(2): 467–480.

# 网状结构 TiB/(TA15-Si)复合材料抗蠕变性能提升及内在机理

王 帅1, 张 芮1, 纪 明1, 孙枫泊1, 麻子硕1, 安 琦1, 黄陆军1,2, 耿 林1,2

- 1. 哈尔滨工业大学 材料科学与工程学院,哈尔滨 150001;
- 2. 哈尔滨工业大学 材料结构精密焊接与连接全国重点实验室,哈尔滨 150001
- 摘 要: 为评估飞机蒙皮用钛基复合材料的高温蠕变性能,采用低能球磨和真空热压烧结技术制备了 TA15 合金 以及具有网状结构的 TiB/TA15 和 TiB/(TA15-Si)复合材料。结果表明,引入 TiB 和 Si 可使合金 600 ℃稳态蠕变率降低 1 个数量级。Si 在 700 ℃时可保持有益效果,而 TiB 的积极作用则由于其附近的孔隙和界面脱粘而减弱。烧结态 TiB/(TA15-Si)复合材料的蠕变变形由位错攀移主导,600 ℃时的高蠕变抗力主要归因于晶界  $\alpha$  相的消除、TiB 晶须的载荷传递以及硅化物对位错运动的阻碍,其在 700 ℃时的低稳态蠕变速率主要来源于晶界  $\alpha$  相的消除以及更多硅化物和  $\alpha$ 2 的动态析出。

关键词: 非连续增强钛基复合材料; TiB 晶须; 网状结构; 硅化物; 蠕变性能